Synthesis, Characterization, and Optical Properties Study of Poly(*o*-aminophenol)/MWCNT Composite

Hajar Ali Hussein[1], Mohammed Qasim Mohammed[1*], and Furat Ahmed Al-Saymari[2]

[1]*Department of Chemistry, College of Education for Pure Science, University of Basrah, Basrah 61004, Iraq*

[2]*Department of Physics, College of Education for Pure Science, University of Basrah, Basrah 61004, Iraq*

* ***Corresponding author:***

email:
mahammed.qasim@uobasrah.edu.iq

Received: February 8, 2025
Accepted: July 23, 2025

DOI: 10.22146/ijc.104558

Abstract: *In this paper, a functionalized multi-walled carbon nanotube (MWCNT) was prepared to be more active. Poly(o-aminophenol) was attached to MWCNT to create POAP:MWCNT nanocomposites using chemical polymerization. The polymerization process occurred in the acidic medium of hydrochloric acid and ammonium persulfate ($(NH_4)_2S_2O_8$) as an oxidizing reagent. The product nanocomposites were characterized via FTIR, XRD, SEM, and TGA. The effects of the addition on the structure, morphology, thermal, electrical, and optical properties of POAP and POAP:MWCNT were investigated. FTIR spectra revealed that carboxylic acid groups formed at the MWCNTs and the nanocomposite. As TGA confirmed, insertions of MWCNT within the polymer matrix led to apparent thermal amelioration. Furthermore, XRD spectra displayed the crystalline nature of POAP and nanocomposite materials. The SEM images of POAP:MWCNT show that the MWCNTs are dispersed within the structure of polymer chains, proving that the POAP:MWCNT composite was successfully prepared. The findings revealed that the electrical conductivity of poly(o-aminophenol) composite thin film was significantly enhanced by about 20000× due to doping by 1 wt.% MWCNT.*

Keywords: *poly(o-aminophenol); POAP:MWCNT composite; optical properties; surface morphology; electrical conductivity*

■ INTRODUCTION

In recent decades, the development processes of organic semiconductors and nanocomposites have attracted considerable attention due to their broad spectrum of promising applications in optoelectronic devices [1]. The nanoparticle fillers generally have a large surface area-to-volume ratio and unique mechanical, electrical, optical, and magnetic features. These particle features usually lead to enhancing the electrical and optical features of materials [2-3].

Chemical functionalization is considered a favored path for improving the dispersion properties of nanocarbon materials [4-5]. Functional groups such as hydroxyl (OH), carbonyl (C=O), and carboxyl (COOH) groups were incorporated within surfaces and walls of nanomaterials by using chemical and physical strategies [6]. One of the most popular functionalization techniques is the chemical oxidation of multi-walled carbon nanotube (MWCNT) due to its modifiability and effectiveness [7]. Nitric acid, hydrogen peroxide, sulfuric acid, and potassium permanganate are considered the most familiar usage reagents for oxidation functionalization [6,8-9]. This chemical functionalization has enabled the modification and insertion of other functional groups within nanosubstrates [10]. The best materials used to manufacture nanocomposites are polymers, including electroactive polymers, which are also known as synthetic metals. The chemical modification of MWCNT probably leads to a sturdy interfacial interaction with many polymer chains, allowing MWCNT-based materials to improve electrical, optical, and functional properties [11-13].

Electroactive polymers are conjugated organic molecules with highly reversible redox merits, environmental stability, electrical conductivity, and

shared properties between plastics and metals. Polymer/nano hybrid composites have synergetic behavior between the polymer and the nanomaterial [14-16]. As one of the effective derivatives of polyaniline, poly(*o*-aminophenol) (POAP) has been prepared widely via chemical oxidative polymerization [17] and electropolymerization [18-19]. POAP has interesting prospects for application in electrocatalytic materials, biochemistry, and electrochemistry [20-21], pH response, chemical sensors, and corrosion protection [22-24]. Electro-active polymers containing two oxidizable groups, such as amine (NH_2) and OH, have attracted the attention of researchers in recent years because they possess electrochemical and optical features similar to those of anilines and phenols. Moreover, the OH group increases the density of imine sites [25]. The present work, POAP and POAP:MWCNT composite, was prepared. The structural characteristics, such as FTIR spectra, XRD patterns, and the topography of the prepared materials, were investigated to reveal that the POAP and POAP:MWCNT were successfully synthesized. The optical and electrical properties of the POAP and POAP:MWCNT thin films were studied and compared.

■ EXPERIMENTAL SECTION

Materials

MWCNT with an outer diameter of 10-30 nm and a purity of approximately 90% were used in this study. Additionally, some acids, such as 37% hydrochloric acid (HCl), 65% nitric acid (HNO_3), and 95% sulfuric acid (H_2SO_4) are purchased from Sigma-Aldrich. Moreover, *o*-aminophenol (Sigma Aldrich), deionized water, *N*-methyl-2-pyrrolidone (NMP), ammonium persulfate (APS, $(NH_4)_2S_2O_8$), and pre-patterned ITO substrates consisting of interdigitated ITO fingers are purchased from Ossila company.

Instrumentation

The following instruments were used: Fourier transform infrared (FTIR) spectrometer, X-ray diffraction (XRD) (Rigaku Ultima IV, Japan), thermogravimetric analysis (TGA, TG-50A Shimadzu, Japan), scanning electron microscope (SEM, TESCAN Mira3, Japan), energy dispersive X-ray (EDX), centrifuge, and a Keithley 2400 Source Meter for measuring I-V characteristics.

Procedure

Modification of MWCNT

One of the most popular MWCNT functionalization techniques is oxidation by adding OH, C=O, and COOH groups, which improve the surface accessibility for further chemical modifications, using oxidizing acid solutions such as HNO_3, H_2SO_4:H_2O_2, or H_2SO_4:HNO_3 that can be used to oxidize MWCNT [14]. Chemical oxidation process was accomplished by using a mixture of 90 mL of H_2SO_4 and 30 mL of HNO_3 in a ratio of 3:1 to avoid the destruction of the nanotubes for 30 min. Next, 0.3 g of MWCNT was added. The mixture was stirred magnetically for 6 h at 50 °C. Then, the product was washed with DI water several times using a centrifuge. Finally, the product was dried at room temperature for 12 h, and the structure of MWCNT is shown in Fig. 1.

Synthesis of POAP

Chemical oxidative polymerization of *o*-aminophenol was accomplished by using *o*-aminophenol as monomer and APS as initiator (in 1:1 molar ratios) in an acidic medium at room temperature. The synthetic procedure is typically summarized in Fig. 2. First, 9 mmol (0.9821 g) of *o*-aminophenol and 1 mL of HCl were added to 60 mL of deionized water. Then, 9 mmol (2.0538 g) of APS in 8 mL of water was added to the mixture drop by drop for 20 min at room temperature. The reaction content was stirred for 72 h at room temperature [10]. At the end of the polymerization, the precipitated dark brown solid was filtered and washed with an excess of deionized water. The product POAP was

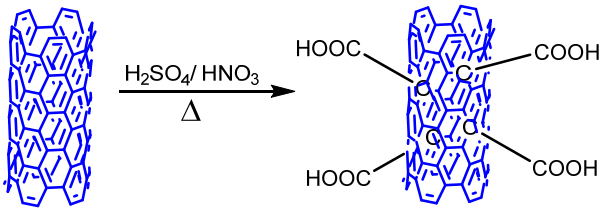

Fig 1. Modification process of MWCNT

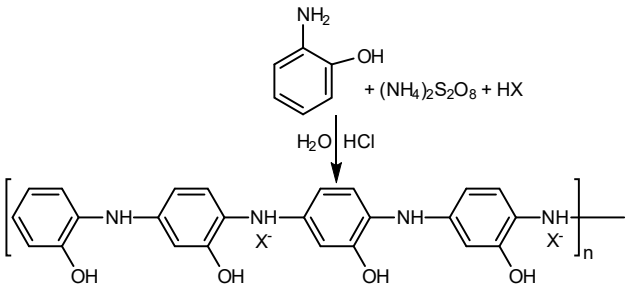

Fig 2. Structure of POAP

dried at 38 °C. Fig. 2 and 3 show the structure and preparation scheme of POAP compound.

Preparation of POAP:MWCNT composites

POAP composite was prepared from a mix of POAP and 1 wt.% MWCNT. In general, the procedure of polymer composite was summarized in Fig. 4. Then, 9 mg of MWCNT was added to the mixture and ultrasonicated at 25 °C for 3 h in an ultrasonic bath. Next, at room temperature, 9 mmol (2.0538 g) of APS in 8 mL of deionized water was added to the above mixture. The reaction mixture was left for 72 h at room temperature [26]. The solid product was collected using centrifugation, washed with deionized water, and dried at 38 °C. Fig. 4 and 5 show the structure and preparation scheme of POAP:MWCNT composite.

Preparation of thin films of POAP and POAP:MWCNT composite for electrical and optical properties

Thin films of homopolymer and composite were synthesized as follows: 0.02 g of *o*-aminophenol and 0.02 g of POAP:MWCNT were dissolved in 2 mL of NMP solvent separately. Both solutions were circulated at 40 °C for 10 min in an ultrasonic bath. Then, each solution was cast onto crosslinked ITO substrates at 40 °C for 3 h.

■ RESULTS AND DISCUSSION

Structural Analysis

FTIR spectroscopy

FTIR was applied to investigate the structures of compounds. Fig. 6 (red curve) shows the FTIR spectrum of the *o*-aminophenol compound. There are some main peaks that can be listed. Two sharp absorption bands show at 3460 and 3273 cm^{-1} in the case of monomer, which could be due to the asymmetrical and symmetrical N–H stretching vibrations of primary amine. A medium absorption band appearing at 3010 cm^{-1} in the case of monomer is attributed to the C–H stretching vibration of the aromatic ring. The peak at 1623 cm^{-1} relates to the C=C stretch of phenyl, and an absorption band appears

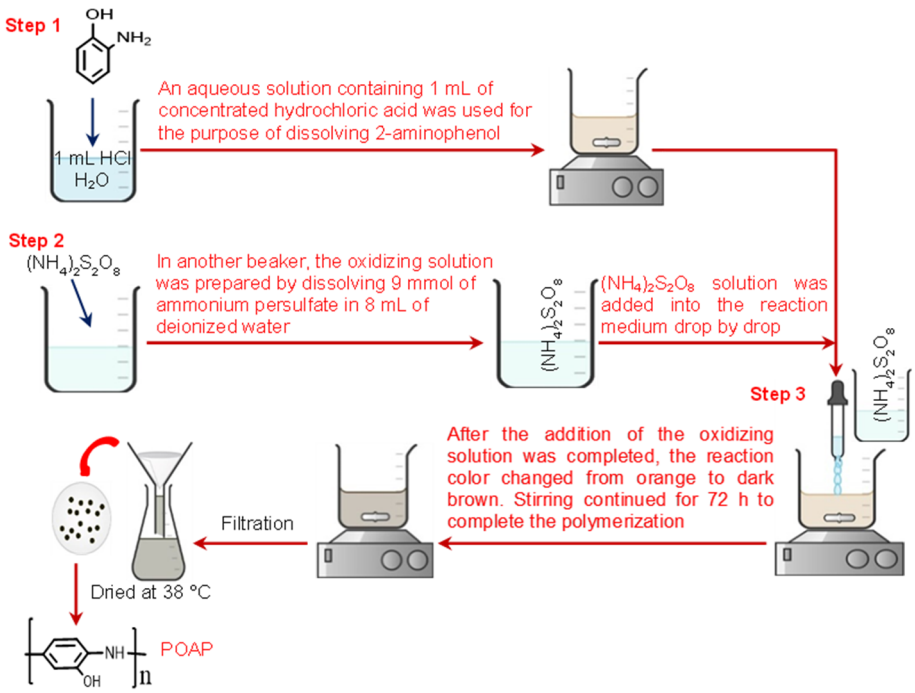

Fig 3. Schematic diagram of polymer POAP preparation steps

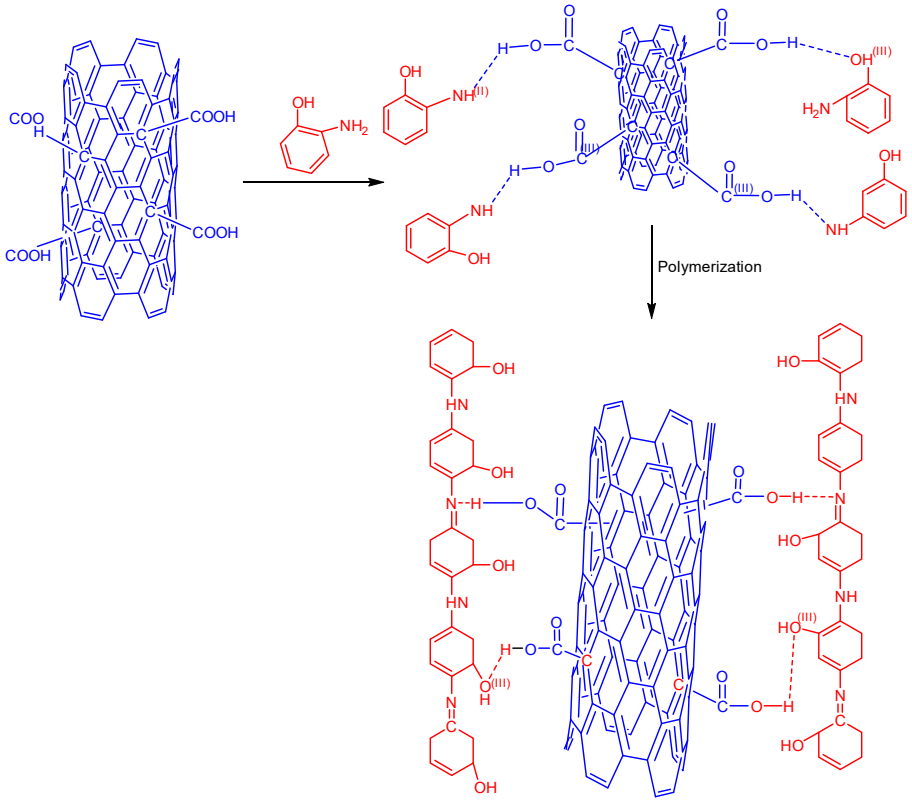

Fig 4. The structure of the POAP:MWCNT composite

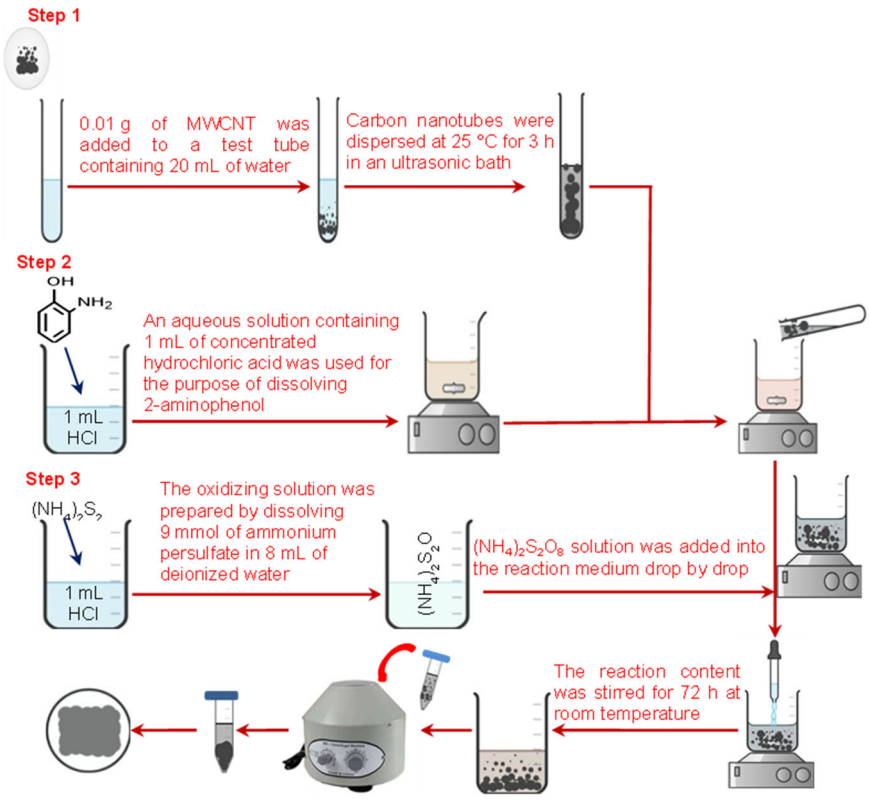

Fig 5. Schematic diagram of POAP:MWCNT preparation steps

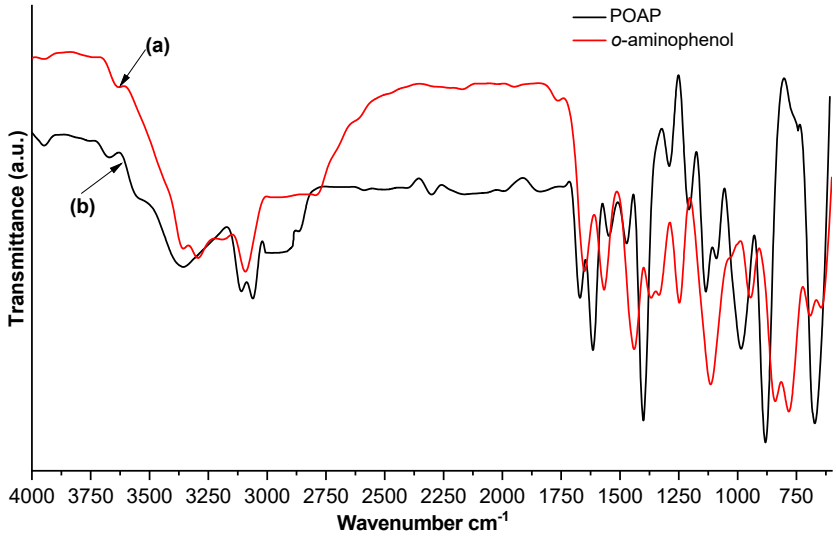

Fig 6. FTIR spectra of (a) *o*-aminophenol, and (b) POAP

at 1525 cm^{-1} as N–H bend. The 1170 to 1107 cm^{-1} peaks corresponded to the C–H out-of-plane bending vibration [27].

FTIR spectrum of the prepared polymer is shown in Fig. 6(b). The spectrum of poly *o*-aminophenol shows a peak at 3320 cm^{-1} due to the characteristic bands of the N–H stretching vibrations. The disappearance of the NH_2 band in the spectrum is observed, proving that the polymerization was achieved via NH_2 groups. Medium peak at 3250 cm^{-1} may be due to the OH stretching vibration. An absorption band appears at 3035 cm^{-1}, attributed to the C–H stretching vibration of the phenyl ring. The peak at 1602 cm^{-1} is associated with the C=C stretching of benzene. The C–N stretching peak is at 1128 cm^{-1}. The peak at 1384 cm^{-1} is clearly seen, which could be assigned to a secondary aromatic amine's C–N stretching vibration. The 1176 to 1043 cm^{-1} peaks correspond to the out-of-plane C–H bending vibration. The bending peak of OH could appear at 970 cm^{-1}.

Fig. 7 shows the comparison between the MWCNT, polymer, and composite spectra. Carboxyl functionalization was confirmed using the FTIR spectrum. In the spectrum of modified MWCNT, an adsorption band due to the –COOH peak at 3358 cm^{-1} was noted. Another peak appears at 2954 cm^{-1}, attributed to symmetric and asymmetric CH_2 stretching. The other weak band at 1745 cm^{-1} represents the carboxylic acid group. Furthermore, the C=O band appeared at 1595 cm^{-1}. The FTIR spectrum of the prepared composite is shown in Fig. 7. A broad absorption peak at 3400 cm^{-1} is observed in the composite spectrum, which is attributed to hydrogen bonding between NH and OH groups in polymer and COOH groups in MWCNT. The absorption band of C=O of the nanotube appears at 1720 cm^{-1}. The peak at 1605 cm^{-1} is associated with C=C stretching of the aromatic ring. The C–N stretching has a peak at 1290 cm^{-1}. The peaks at around 1184 to 1116 cm^{-1} correspond to the out-of-plane bending vibration of C–H. The FTIR spectrum of the polymer contains peaks at 3320, 3250, 3035, and 1602 cm^{-1} due to the characteristic bands of the N–H, –OH, C–H, and C=C stretching vibrations.

Thermal characterization

TGA analysis was applied to estimate the thermal stability of the polymer and composite POAP:MWCNT. Fig. 8 displays the TGA curve of POAP. The polymer was degraded in three stages; the first stage of thermal degradation was found in the 41–190 °C range, probably due to the loss of water molecules in polymer chains. The second stage is 225–350 °C with a weight loss of 23%, related to the depolymerization of aminophenol chains, vaporization, and elimination of volatile product moieties. The third stage is shown at around 355–595 °C with a weight loss of 35.5%, which may be due to the breaking of weak bonds of polymer chains, elimination of volatile products, and conversion to small molecules

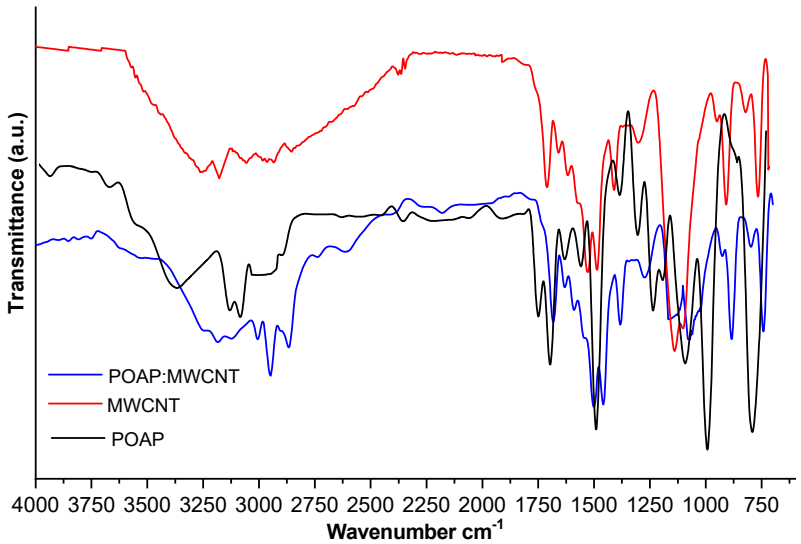

Fig 7. FTIR spectra of POAP, MWCNT, and POAP:MWCNT composite

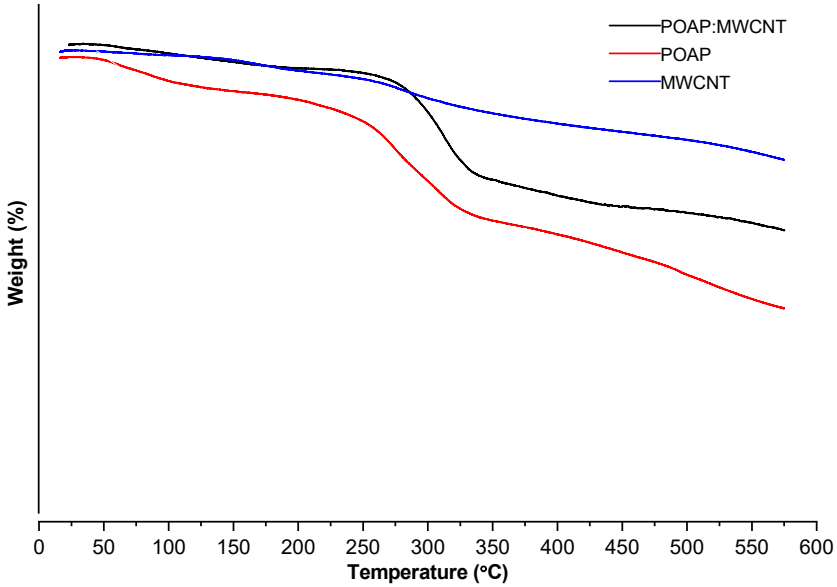

Fig 8. The TGA curve of MWCNT, POAP, and POAP:MWCNT composite

and carbonic residue. The weight losses of the original POAP at the end of decomposition were 35.5% at 600 °C.

The thermal decomposition curves of composite POAP:MWCNT showed three stages. The degradation temperature for the first stage is about 5% weight loss in the 40–190 °C range, probably due to the loss of water molecules in polymer chains. The second stage is 200–345 °C with a weight loss of 18%, related to the depolymerization of polymer chains, and elimination of volatile product moieties. The third stage is around 350–585 °C with a weight loss of 24%, which may be due to breaking bonds of polymer chains, eliminating volatile products, and converting to small molecules. The total weight loss of poly aminophenol from its original weight at the end of decomposition was found to be 24% at 600 °C. These results indicated that nanocarbon enhanced the thermal stability of polymers due to the interaction between nanotubes and polymer chains [28]. TGA curves for MWCNT typically show a progressive weight loss at high temperatures. The TGA curve of MWCNT–COOH shows that almost no weight loss occurs for the MWCNT when the temperature is

increased to 570 °C. Weight starts to be lost at about 250 °C, with a total loss of about 12 wt.% at the temperature of 570 °C. Generally, MWCNTs dispersed within the polymer chains act as a physical barrier to the diffusion of volatile gases, small molecules, and oxygen. This effect delays the thermal decomposition process. Furthermore, MWCNTs have a high thermal conductivity, which can help dissipate heat more efficiently throughout the polymer composite and prevent localized "hot spots". Also, MWCNT can act as radical scavengers, reacting with and stabilizing free radicals generated during decomposition. In addition, the large surface area of MWCNT permits strong physical interactions with the polymer matrix.

XRD patterns

The XRD patterns of the MWCNT, POAP, and POAP:MWCNT are shown in Fig. 9. The composite film shows similar peaks to those of the polymer. However, this peak in composite was weaker than that of pure polymer, indicating the interaction between POAP and MWCNT. The crystallinity of the polymer was good because of the hydrogen bonding between polymer molecules. Typical (002) and (100) peaks of MWCNT appear at 2θ of 25.5° and 43°, respectively, which is in agreement with the previous studies. The diffraction pattern of the polymer has the distinctive peaks at 2θ of 12°, 15°, 25°, and 29°. The composite's XRD patterns indicates the appearance of almost the same peaks in the polymer and the MWCNT, with a difference in intensity due to the interference between them [29]. The degree of crystallinity is estimated from the area of crystalline peaks and the location of amorphous peaks. The degree of crystallinity of nanotubes, polymer, and nanocompounds is equal to 96.9, 89.4, and 92.9%, respectively [30].

SEM measurements

From Fig. 10(a1) and 10(a2), the SEM images of MWCNT exhibit that there are small bundles of MWCNT, each other, which were looked crosslinked and incompact. SEM also investigated the prepared POAP's structural characterization, and this polymer's topography is shown in Fig. 10(b1) and 10(b2), exhibiting many pieces with dimensions of about hundreds of nanometers. Additionally, from the SEM images of POAP:MWCNT

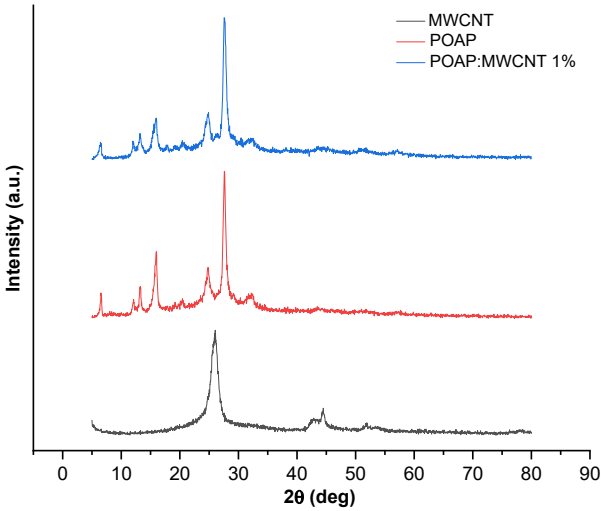

Fig 9. The XRD pattern of MWCNT, POAP, and POAP:MWCNT composite

composite (Fig. 10(c1) and 10(c2)), it can be noticed that the MWCNTs are dispersed within the structure of polymer chains, revealing that the POAP:MWCNT composite was successfully synthesized.

Moreover, the size of the nanotube, polymer, and nancomposite materials are detected by calculating the average size of particles in SEM images, as shown (Fig. 11). The size of particles in the composites was determined using the ImageJ software program. After acquiring the measurement data, they were entered into Origin software to obtain the average size, analyze the size distribution, and prepare the relevant graphs. These compounds displayed an average of 38.65, 349.79, and 590.82 nm, respectively. The nano dimensions assist in creating the connections and arrangements of the polymer matrix. In general, these nanoparticles' presence supports the nanocomposite's electrochemical behavior.

To allow for the qualitative detection of polymer nanocomposites and demonstrate the increase of carbon ratio in the polymer composite, EDX measurement was achieved. The polymer matrices were analyzed after inserting nanotubes using EDX measurements. Fig. 12(a) and 12(b) depict EDX spectra of the polymer before and after insertion of nano, respectively. The findings indicate the presence of nanoparticles within the polymer matrices due to the bonding between the nano and polymer chains. EDX measurements can strongly reference the existence of nanoparticles in a polymer matrix. EDX can

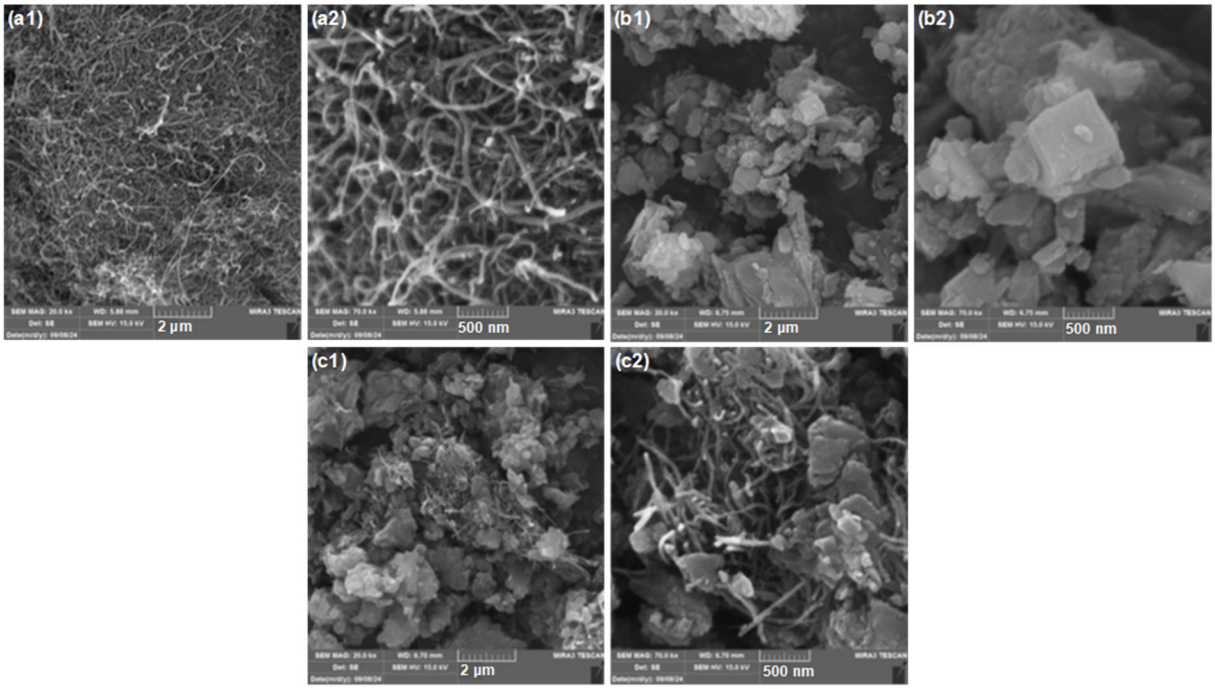

Fig 10. SEM images of (a) MWCNT, (b) POAP, and (c) POAP:MWCNT composite

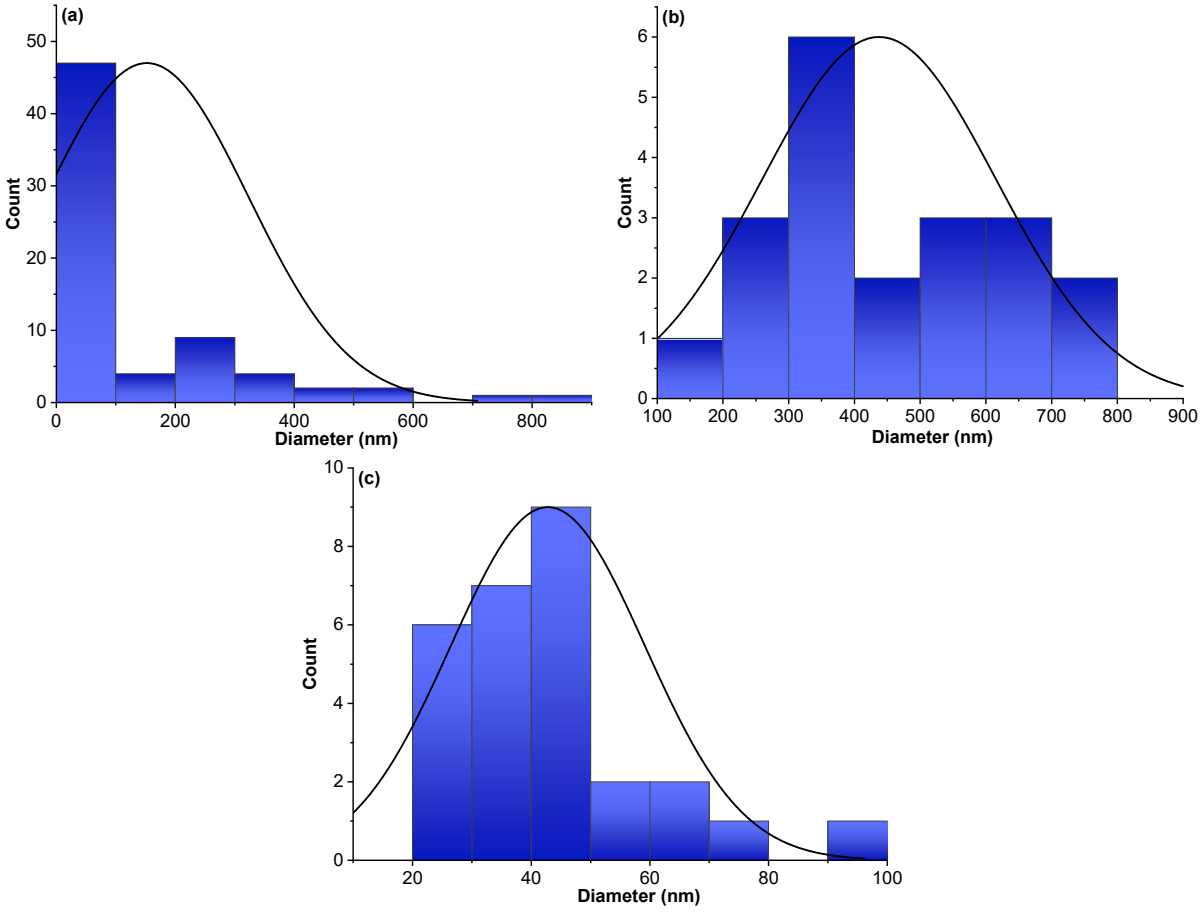

Fig 11. The histogram distribution of nanoparticles in the (a) MWCNT, (b) POAP, and (c) POAP:MWCNT composite

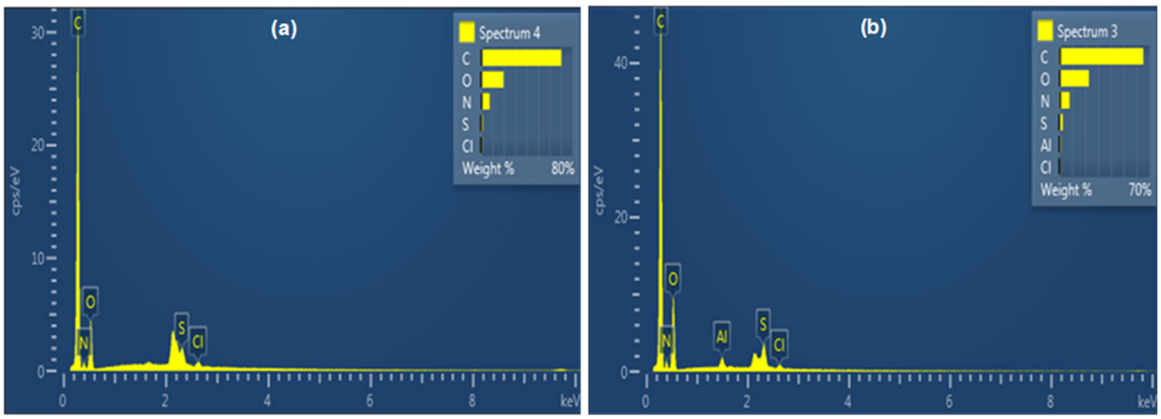

Fig 12. The EDX images of (a) POAP and (b) POAP:MWCNT

provide semi-quantitative information about the relative abundance of elements. This can help to observe changes in concentration across different areas of the sample. In this study, both polymer and composite contain carbon and oxygen. From a comparison between two curves, it can be noted that there is no apparent difference in the carbon peak. However, a notable oxygen peak higher than what would be seen in the pure polymer matrix alone is crucial for confirming the existence of MWCNT–COOH nanoparticles in the polymer matrix.

Linear Optical Properties of POAP and POAP:MWCNT Composite

In order to evaluate the linear optical properties of the POAP and POAP:MWCNT, the absorption and reflectivity spectra of the thin films were measured using a double beam UV-vis spectroscopy, Shimadzu Scientific Instruments Incorporated, Japan. Some of the optical constants such as absorption coefficient α, extension coefficient k, optical energy gap E_g, refractive index n, dielectric constant ε, static dielectric constant ε_s, lattice dielectric constant ε_∞, and static reflective index n_s.

Absorption and reflectance spectra of POAP and POAP:MWCNT thin films

The absorption (A) and reflectance (R) spectra of the prepared thin films were measured as a function of wavelength at room temperature and plotted in Fig. 13. It can be noticed that the absorption spectrum of the two samples exhibited a peak at around 300 nm, attributed to the transition n-π*, and when the wavelength increases (λ > 300 nm), the absorbance of the thin films decreases (see Fig. 13(a)). The results show that the absorbance of the POAP:MWCNT thin film is slightly higher than that of the pure polymer. In addition, both samples show a low reflectivity, around 5.5% (for λ > 350 nm), and when the wavelength decreases, the reflectivity decreases to ~4% at around 300 nm. While, the reflectance spectrum of the POAP:MWCNT thin film

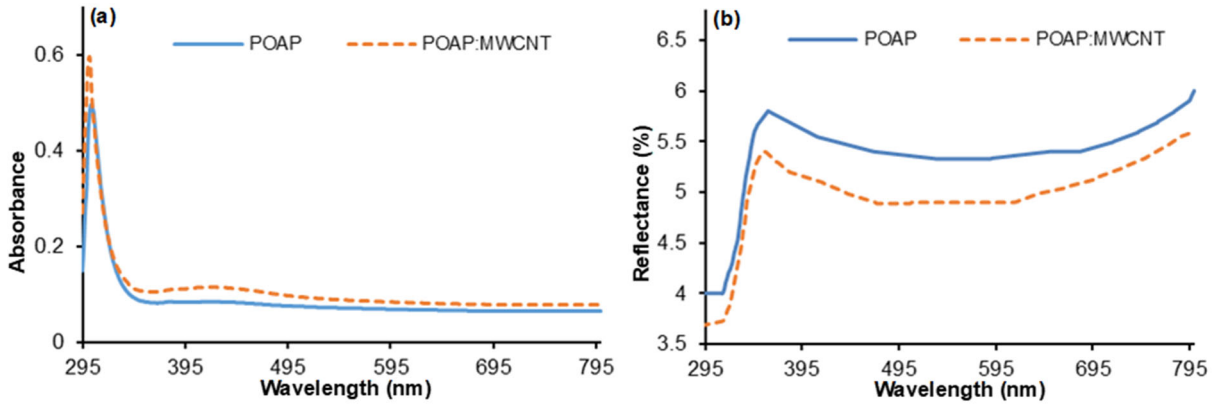

Fig 13. (a) The absorbance and (b) reflectance spectra of POAP and POAP:MWCNT thin films

shows relatively lower reflectivity, it is about 5% (for λ > 350 nm). When the wavelength decreases, the reflectivity decreases to 3.5% at ~300 nm.

The enhancement in absorption of the organic materials doped with MWCNT is due to a combination of factors, such as increasing the surface area of the material, improving charge carrier transfer, and inducing polarization effects [31-33]. The cylindrical structure and the high aspect of the dopant material (MWCNT) strongly interact with light and significantly increase the organic material's conjugation length (increase the composite material's surface area), acting as a light-pathway within the organic material. The large surface area of the composite and the ability of MWCNT to act as a light-pathway provide the interaction between the light and the organic molecules, leading to enhance absorption and decreasing the transmittance [34-35]. MWCNT could also act as a conductivity bridge, causing an increase in the charge carriers (electrons and holes) and an enhancement in the charge transport within the organic material. Consequently, the radiative recombination process is optimized; increasing the absorption [36]. Additionally, the interface between the organic material and MWCNT could create polarization effects when the composite material is exposed to light. These effects could enhance the energy dissipation and absorption [33,37].

Absorption coefficient and optical energy gap of POAP and POAP:MWCNT thin films

The absorption coefficient α could be obtained from the absorbance A using Eq. (1) [38];

$$\alpha = 2.303\frac{A}{d} \quad (1)$$

where d is the thickness of the thin films (~300 nm). Fig. 14(a) shows the prepared thin films' absorption coefficient as a function of wavelength. It can be seen that both samples have high values of α (> 10^4 cm^{-1}) at around 300 nm, allowing direct electronic transitions (direct energy gap). To calculate the optical energy gap E_g, the Tauc formula was used, which is related to α by Eq. (2) [39];

$$(\alpha h\nu)^{1/w} = q\left(h\nu - E_g\right) \quad (2)$$

where h is Planck's constant, w = 0.5 (for α > 10^4), ν is the light frequency, and q is a constant. To evaluate the value of E_g, $(\alpha h\nu)^2$ was plotted as a function of hν (see Fig. 14(b)), and the band gap could be determined by intersecting the tangent to each curve with the x-axis. The E_g value was estimated at 3.94 eV for both samples, POAP and POAP:MWCNT thin films. This is attributed to the fact that the energy gap calculated in the present work is the optical energy gap, which can be determined from the absorption spectrum using the Tauc plot method. Doping organic materials with MWCNT could influence the absorption spectrum and the electronic structure of this material by introducing new energy levels within the energy gap. However, if the absorbance spectrum of organic material (undoped) and the composite (doped material) are similar, then the absorbance characteristics are also identical. As shown in Fig. 13(a), the POAP:MWCNT nanocomposites exhibit a similar absorbance spectrum to that of the undoped.

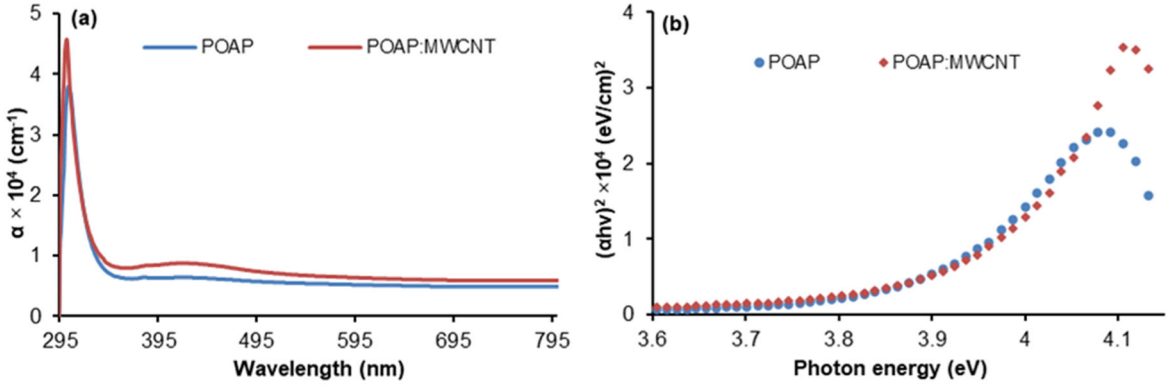

Fig 14. (a) The absorption coefficient α and (b) $(\alpha h\nu)^2$ against light energy (hν), for POAP and POAP:MWCNT thin films

This is attributed to the absorption of dopant material (MWCNT) that show intensity peak around 310 nm, as reported in the previous study [40], which is very close to that of the POAP material, thereby, applying Tauc plot method which is derived from UV-visible absorption data show that both materials have approximately similar values of the energy gap.

The extinction coefficient, refractive index, and dielectric constant of POAP and POAP:MWCNT

Extinction coefficient (k) represents the material's ability to interact (absorb) with incident light. A high k in composite materials indicates that the blending material exhibits a strong optical absorption, which is vital for photo-applications such as solar cells and photodetectors. The k is related to the absorption coefficient α using Eq. (3) [41];

$$k = \frac{\lambda\alpha}{4\pi} \tag{3}$$

Fig. 15(a) shows the k as a function of wavelength of the prepared thin films, exhibiting a peak at around 300 nm corresponding to high absorption at that wavelength. It was also observed that for λ > 360 nm, the k values are nearly constant. It was also found that doping POAP polymer with MWCNT increases the k of the organic material due to enhanced absorption and scattering of light and improves the dispersion of MWCNT within the organic matrix. Thus, the interaction between the composite material and light is enhanced, resulting in a higher k [42-43].

Refractive Index (n), which measures how the light propagates through a material, and when the mixed material generates a high n, suggests better light confinement, essential for optical devices like waveguides or sensors. However, a mismatched n between the matrix and pitches in a composite can lead to scattering or reflection [44]. The n of the thin films was determined using Eq. (4).

$$n = \frac{1+R}{1-R} + \sqrt{\frac{4R}{(1+R)^2} - k^2} \tag{4}$$

As seen from Fig. 15(b), for λ > 350 nm, the n of POAP and POAP:MWCNT thin films polymer is estimated to be around 1.63 and 1.59, respectively. It was also observed that, for λ < 350, the n values decrease with decreasing wavelength to around 1.5 for the undoped polymer and 1.74 for the doped sample. The result shows

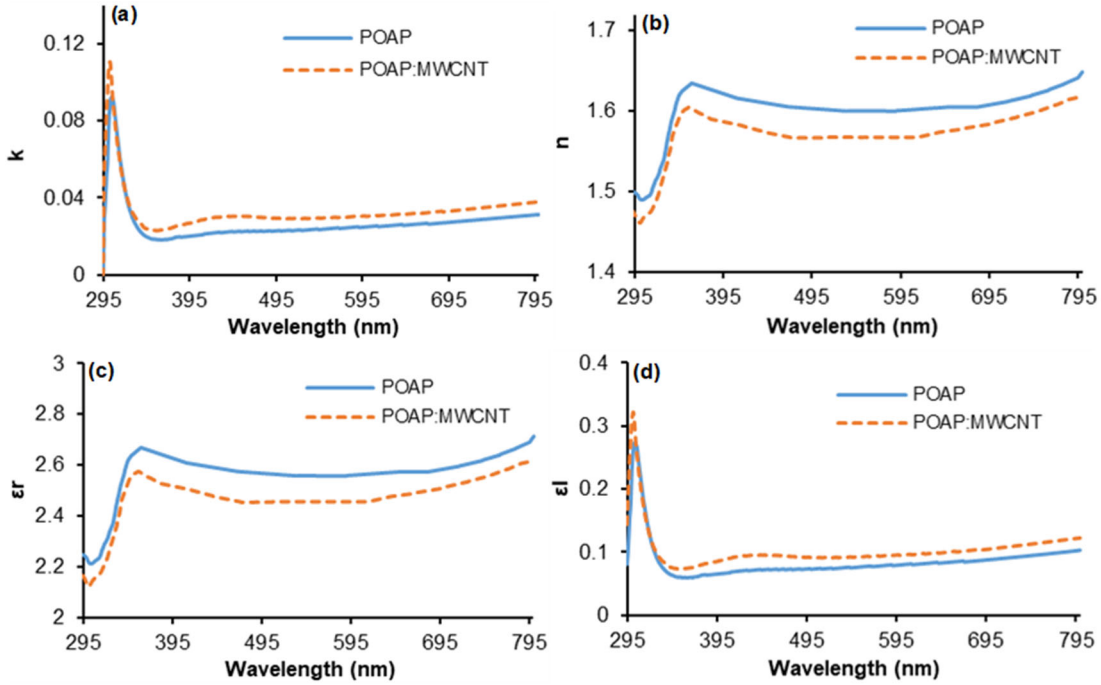

Fig 15. (a) Extinction coefficient k, (b) refractive index n, (c) real dielectric constant, and (d) imaginary dielectric constant as a function of wavelength for POAP and POAP:MWCNT thin films

that doping the pure polymer with MWCNT decreases the n value. This is because when the organic material is doped with MWCNT, the charge transport is enhanced and the number of charge carriers increases. Thus, when the composite material is exposed to light, these additional charge carriers could absorb more incident photons, enhancing the absorption (reduction in transmittance) and decreasing the n value [45-46].

The dielectric constant reveals the material's ability to store electrical energy in the presence of an electric field, and its high value indicates a higher degree of polarizability, which contributes to better charge separation and storage. This parameter can be influenced by the blending material's nature, interfacial polarization, and dispersion [47]. The real and imaginary parts of the dielectric constant (ε_r and ε_I) are related to the refractive index and extinction coefficient by Eq. (5) and (6) [48].

$$\varepsilon_r = n^2 - k^2 \quad (5)$$

$$\varepsilon_I = 2nk \quad (6)$$

The real and imaginary dielectric parts were determined as a function of wavelength and plotted in Fig. 15(c) and 15(d). It can be seen from these results that the behaviors of ε_r and ε_I are similar to those of reflectivity and absorbance spectra, respectively. Fig. 15(c) shows that when the POAP polymer is doped with MWCNT, the dielectric constant increases due to the high conductivity of MWCNT and consequently enhanced polarization effects at the interface between the polymer matrix and MWCNT. The MWCNT act as conductive pathways within the polymer, enhancing the charge accumulation at the interface between the polymer and MWCNT. This enhancement leads to an increase in the polarization and the dielectric constant [49].

Cauchy and the single-effective-oscillator models

The n is related to the wavelength of the incident light by Eq. (7) [35];

$$n = C_1 + \frac{C_2}{\lambda_2} \quad (7)$$

where C_1 and C_2 are Cauchy parameters (constants). To estimate the values of these two parameters, the n of the prepared thin films was plotted as a function of $1/\lambda^2$ (see Fig. 16(a)). By fitting the linear variation in the two curves, C_2 and C_1 could be obtained from the slope and the intercept with the vertical axis, respectively. Table 1 lists the values of Cauchy parameters and the static dielectric constant ε_s, which is related to C_1, where $\varepsilon_s \approx C_1^2$.

The single-effective-oscillator energy (E_0) and dispersion energy (E_d) of the prepared thin films could be determined from the single-effective-oscillator model (Wemple-DiDomenico model), which is given by Eq. (8) [36];

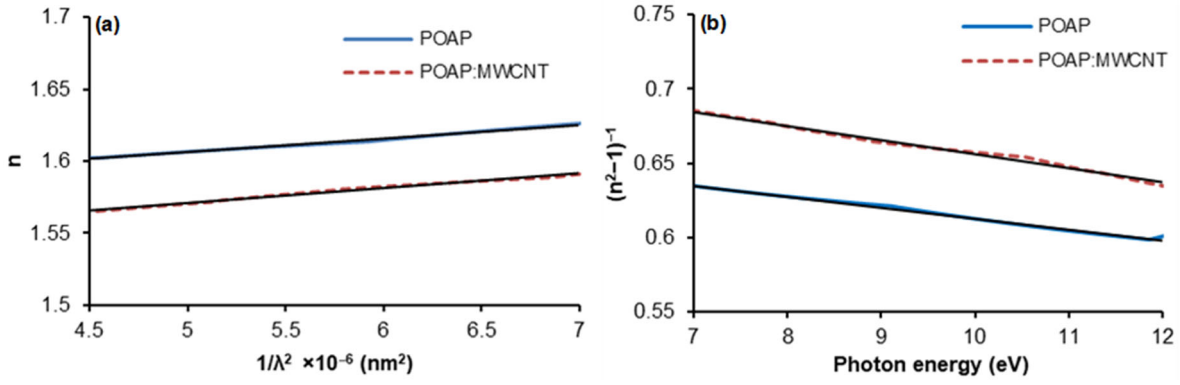

Fig 16. Refractive index as a function of (a) $1/\lambda^2$ and (b) $(n^2 - 1)^{-1}$ as a function of incident photon energy for POAP and POAP:MWCNT thin films

Table 1. Opto-electronic parameters of POAP and POAP:MWCNT thin films

Sample	E_g (eV)	n	C1	C2 (nm^{-2})	ε_s	E_0 (eV)	E_d (eV)	n_s
POAP	3.94	1.63	1.56	9300	2.43	8.8	12.2	1.544
POAP:MWCNT	3.94	1.59	1.52	10400	2.31	8.4	11.3	1.531

$$n^2 - 1 = \frac{E_0 E_d}{E_0^2 - E^2} \quad (8)$$

where E is the photon energy (hν). This expression could be written as in Eq. (9).

$$\left(n^2 - 1\right)^{-1} = \frac{E_0}{E_d} - \frac{E}{E_0 E_d} \quad (9)$$

The values of E_0 and E_d are obtained from the slope and intercept with the vertical axis of the linear variation in the $(n^2 - 1)^{-1}$ as a function of photon energy (E) (see Fig. 16(b)). The static refractive index n_s was evaluated by extrapolating the single-effective-oscillator model at E = 0 using Eq. (10);

$$n_s^2 = 1 + E_d / E_0 \quad (10)$$

The values of E_0, E_d, and n_s of the POAP and POAP:MWCNT thin films are listed in Table 1.

Electrical Properties of POAP and POAP:MWCNT Thin Films

To investigate the electrical properties of the prepared thin films, POAP and POAP:MWCNT were deposited on the interdigitated ITO substrates using the casting method. The current-voltage (I-V) characteristics of the prepared thin films were measured at room temperature and plotted in Fig. 17. The electrical current of POAP thin film was enhanced by a factor of 20000× due to doping by MWCNT (1 wt.%). The electrical conductivity of the POAP and POAP:MWCNT thin films is 0.5×10^{-6} S/cm and 0.1 S/cm, respectively. Several studies have shown that doping organic semiconductor materials with MWCNT could significantly enhance their electrical current and conductivity [50-51]. This enhancement is attributed to the ability of MWCNTs to act as conductive bridges between polymer chains, thereby improving interchain connectivity and facilitating charge transport. As a result, the mobility of charge carriers within the organic material is optimized, leading to an increase in the number of charge carriers and, consequently, improved electrical performance [52-53].

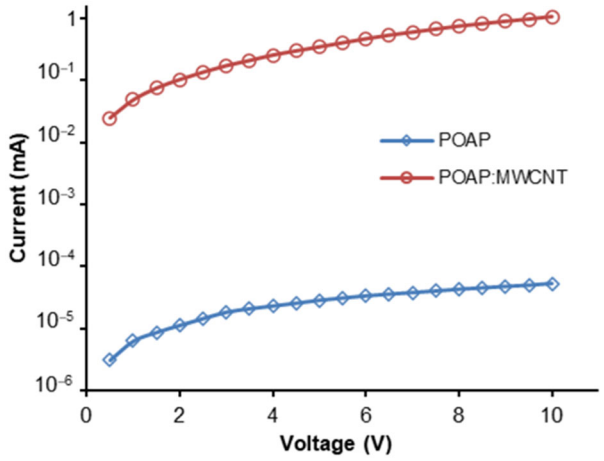

Fig 17. Room-temperature current-voltage characteristics for POAP and POAP:MWCNT thin films under dark conditions

■ CONCLUSION

POAP and POAP:MWCNT composite were successfully prepared. The FTIR spectra of compounds have shown good evidence for preparing a polymer and a composite. TGA results indicated that nanocarbon enhanced the thermal stability of polymers due to the interaction between nanotubes and polymer chains. XRD patterns of polymer and composite indicated the same peaks in the polymer and the polymer/MWCNT, with a difference in intensity due to the interference. Moreover, from SEM images, it can be noticed that the MWCNT are dispersed within the structure of polymer chains, revealing that the POAP:MWCNT composite was successfully synthesized. Furthermore, the electrical measurements of the POAP and POAP:MWCNT thin films indicate that the conductivity of POAP thin films was significantly optimized due to adding MWCNT as a dopant, exhibiting a superior enhancement by a factor of ~20000×.

■ ACKNOWLEDGMENTS

The authors gratefully acknowledge the Department of Chemistry and the Department of Physics, College of Education for Pure Science, for their assistance.

■ CONFLICT OF INTEREST

The authors declare that there is no conflict of interest regarding the publication of this paper.

■ AUTHOR CONTRIBUTIONS

All authors contributed to the study conception and design. Material preparation, data collection, and

analysis were performed by Hajar Ali Hussein and Mohammed Qasim Mohammed. Some data collection and analysis were performed by Furat Ahmed Al-Saymari. The first draft of the manuscript was written by Hajar Ali Hussein and Mohammed Qasim Mohammed. All authors commented on previous versions of the manuscript, read and approved the final manuscript.

■ REFERENCES

[1] Abdelazeez, A.A.A., Rabia, M., Hasan, F., Mahanta, V., and Adly, E.R., 2024, Polymer nanocomposites: Catalysts for sustainable hydrogen production from challenging water sources, *Adv. Energy Sustainability Res.*, 5 (10), 2400077.

[2] Ismail, H.K., Alesary, H.F., and Mohammed, M.Q., 2019, Synthesis and characterisation of polyaniline and/or MoO_2/graphite composites from deep eutectic solvents via chemical polymerization, *J. Polym. Res.*, 26 (3), 65.

[3] Ngadiwiyana, N., Prasetya, N.B.A., Gunawan, G., Kusworo, T.D., and Susanto, H., 2021, Synthesis, characterization, and study of proton exchange polymer membrane properties of sulfonated copolymer eugenol-diallyl phthalate, *Indones. J. Chem.*, 21 (1), 168–178.

[4] Díez-Pascual, A.M., 2021, Chemical functionalization of carbon nanotubes with polymers: A brief overview, *Macromol*, 1 (2), 64–83.

[5] Thi Mai Hoa, L., 2018, Characterization of multi-walled carbon nanotubes functionalized by a mixture of HNO_3/H_2SO_4, *Diamond Relat. Mater.*, 89, 43–51.

[6] Dubey, R., Dutta, D., Sarkar, A., and Chattopadhyay, P., 2021, Functionalized carbon nanotubes: Synthesis, properties and applications in water purification, drug delivery, and material and biomedical sciences, *Nanoscale Adv.*, 3 (20), 5722–5744.

[7] De Luca, P., Siciliano, C., Macario, A., and Nagy, J.B., 2021, The role of carbon nanotube pretreatments in the adsorption of benzoic acid, *Materials*, 14 (9), 2118.

[8] Speranza, G., 2021, Carbon nanomaterials: Synthesis, functionalization and sensing applications, *Nanomaterials*, 11 (4), 967.

[9] Ramachandran, K., Boopalan, V., Bear, J.C., and Subramani, R., 2022, Multi-walled carbon nanotubes (MWCNTs)-reinforced ceramic nanocomposites for aerospace applications: A review, *J. Mater. Sci.*, 57 (6), 3923–3953.

[10] Zhan, J., Lei, Z., and Zhang, Y., 2022, Non-covalent interactions of graphene surface: Mechanisms and applications, *Chem*, 8 (4), 947–979.

[11] Sharma, S., Sudhakara, P., Omran, A.A.B., Singh, J., and Ilyas, R.A., 2021, Recent trends and developments in conducting polymer nanocomposites for multifunctional applications, *Polymers*, 13 (17), 2898.

[12] Wang, X., Xu, Y., Li, Y., Li, Y., Li, Z., Zhang, W., Zou, X., Shi, J., Huang, X., Liu, C., and Li, W., 2021, Rapid detection of cadmium ions in meat by a multi-walled carbon nanotubes enhanced metal-organic framework modified electrochemical sensor, *Food Chem.*, 357, 129762.

[13] Su, X., Wang, R., Li, X., Araby, S., Kuan, H.C., Naeem, M., and Ma, J., 2022, A comparative study of polymer nanocomposites containing multi-walled carbon nanotubes and graphene nanoplatelets, *Nano Mater. Sci.*, 4 (3), 185–204.

[14] Namsheer, K., and Rout, C.S., 2021, Conducting polymers: A comprehensive review on recent advances in synthesis, properties and applications, *RSC Adv.*, 11 (10), 5659–5697.

[15] Tuma Albaaj, L.T., and Mohammed, M.Q., 2024, Schiff bases and their polymer resins in aqueous solutions: An analytical and adsorption efficiency study, *Acta Chem. Iasi*, 32 (1), 55–72.

[16] Tundwal, A., Kumar, H., Binoj, B.J., Sharma, R., Kumar, G., Kumari, R., Dhayal, A., Yadav, A., Singh, D., and Kumar, P., 2024, Developments in conducting polymer-, metal oxide-, and carbon nanotube-based composite electrode materials for supercapacitors: A review, *RSC Adv.*, 14 (14), 9406–9439.

[17] Kadhim, S.J., Mohammed, M.Q., and Al-Shawi, J.M.S., 2022, An electrochemical sensor for paracetamol and metronidazole detection based on

poly (Schiff bases) film modified electrode, *Eur. Chem. Bull.*, 11 (7), 15–22.

[18] Mohammed, M.Q., Jassem, A.M., Al-Shawi, J.M.S., and Alesary, H.F., 2020, Comparative electrochemical behavior of poly (3-aminobenzoic acid) films in conventional and non-conventional solvents, *AIP Conf. Proc.*, 2290 (1), 030029.

[19] Sonika, S., Verma, S.K., Saha, J., Alsharabi, R.M., and Rajput, S., 2022, Microarticstructural, spectroscopic, and magnetic analysis of multiwalled carbon nanotubes embedded in poly (*o*-aminophenol) matrices, *Adv. Mater. Sci. Eng.*, 2022 (1), 5437954.

[20] Al-Hossainy, A.F., and Zoromba, M.S., 2021, Fabrication, characterization and optical properties of poly(*p*-phenylenediamine-co–*o*-aminophenol) nanostructure thin film, *Appl. Phys. A*, 127 (4), 278.

[21] Hao, Z., Hu, L., Yan, R., Pei, L., and Mo, S., 2024, Sensitive fluorescent detection of *o*-aminophenol by hemicyanine boronic acid, *Spectrochim. Acta, Part A*, 304, 1386–1425.

[22] Yahaya, S.M., Harun, M.K., Ismail, I., and Rosmamuhamadani, R., 2021, Corrosion inhibition of mild steel by electrodeposited poly(m-aminophenol) coating, *Solid State Phenom.*, 317, 498–505.

[23] Buckey, G., Owens, O.E., Gabriel, A.W., Downing, C.M., Calhoun, M.C., and Cliffel, D.E., 2022, Adsorption and electropolymerization of *p*-aminophenol reduces reproducibility of electrochemical immunoassays, *Molecules*, 27 (18), 6046

[24] Ozyilmaz, A.T., 2021, Synthesis of poly (aniline-co-*o*-anisidine) film in electrolyte mixture and its anticorrosion behavior, *Nat. Eng. Sci.*, 6 (3), 197–207.

[25] Godarzi, F., Shi, H., and Arjomandi, J., 2021, Novel poly(*p*-aminophenol-*o*-phenylenediamine)/zinc oxide nanocomposites growth on gold electrode: *In-situ* spectro-electrochemistry and kinetic study, *Synth. Met.*, 274, 116722.

[26] Ahmadi, H., Haddadi-Asl, V., Kowsari, E., and Mohammadi, N., 2022, Pseudocapacitive performance of a ternary composite of ferrocene-functionalized graphene nanoribbon, dicationic ionic liquid, and poly (*o*-aminophenol) for supercapacitor application, *J. Alloys Compd.*, 927, 167021.

[27] Sharanakumar, T.M., Mounesh, M., Praveen Kumar, N.Y., Reddy, K.R.V., and Sunilkumar, A., 2023, Determination of *o*-aminophenol by novel Co(II) phthalocyanine with appliance of composite MWCNTs, *Electrocatalysis*, 14 (3), 381–392.

[28] Feyzi-barnaji, B., Barin, S.M., Mohammadi, A., Naeemy, A., and Darbasizadeh, B., 2023, Voltammetric detection of clopidogrel in pharmaceuticals utilizing electropolymerized *o*-aminophenol-MWCNTs modified electrode, *Russ. J. Electrochem.*, 59 (11), 930–940.

[29] Mallakpour, S., and Madani, M., 2015, *p*-Amino phenol immobilized on multi-walled carbon nanotubes for the preparation of chitosan nanocomposites, *J. Compos. Mater.*, 50 (3), 403–411.

[30] Verma, S.K., Kar, P., Yang, D.J., and Choudhury, A., 2015, Poly(*m*-aminophenol)/functionalized multi-walled carbon nanotube nanocomposite based alcohol sensors, *Sens. Actuators, B*, 219, 199–208.

[31] Urtekin, G., and Aytac, A., 2021, The effect of multi-walled carbon nanotube additives with different functionalities on the properties of polycarbonate/poly(lactic acid) blend, *J. Polym. Res.*, 28 (5), 180.

[32] Huang, X., Liu, X., Jia, Z., Wang, B., Wu, X., and Wu, G., 2021, Synthesis of 3D cerium oxide/porous carbon for enhanced electromagnetic wave absorption performance, *Adv. Compos. Hybrid Mater.*, 4 (4), 1398–1412.

[33] Zhang, F., Jia, Z., Zhou, J., Liu, J., Wu, G., and Yin, P., 2022, Metal-organic framework-derived carbon nanotubes for broadband electromagnetic wave absorption, *Chem. Eng. J.*, 450, 138205.

[34] Wen, B., Zhang, J., Yang, G., Jing, D., Yin, X., Fan, L., Salman Nasir, M., and Ding, S., 2022, Optimal electrical conductivity and interfacial polarization induced by loaded nanoparticles on carbon nanotubes for excellent electromagnetic wave

absorption performance, *J. Colloid Interface Sci.*, 626, 759–767.

[35] Hou, W., Liao, Q., Wu, M., Liao, K., Song, Y., and Qin, L., 2023, High-performance pinecone-like MOF derivative electromagnetic wave-absorbing composite via *in situ* anisotropic-oriented growth, *J. Alloys Compd.*, 937, 168283.

[36] Fikri, M.A., Pandey, A.K., Samykano, M., Kadirgama, K., George, M., Saidur, R., Selvaraj, J., Abd Rahim, N., Sharma, K., and Tyagi, V.V., 2022, Thermal conductivity, reliability, and stability assessment of phase change material (PCM) doped with functionalized multi-wall carbon nanotubes (FMWCNTs), *J. Energy Storage*, 50, 104676.

[37] Guo, Y., Zhu, Y., Sun, J., Lin, Y., Li, X., Liu, G., Gong, Y., Zhang, X., Tian, X., Li, X., and Chen, L., 2025, MOF-derived carbon nanotube bridged Co/MoC@NC composites for enhanced electromagnetic wave absorption, *J. Alloys Compd.*, 1010, 177346.

[38] Jonnalagadda, M., Prasad, V.B., and Raghu, A.V., 2021, Synthesis of composite nanopowder through Mn doped ZnS-CdS systems and its structural, optical properties, *J. Mol. Struct.*, 1230, 129875.

[39] Wang, S., Xu, Y., Chen, T., Jiang, W., Liu, J., Zhang, X., Jiang, W., and Wang, L., 2021, A red phosphor $LaSc_3(BO_3)_4:Eu^{3+}$ with zero-thermal-quenching and high quantum efficiency for LEDs, *Chem. Eng. J.*, 404, 125912.

[40] Zeinabad, H.A., Zarrabian, A., Saboury, A.A., Alizadeh, A.M., and Falahati, M., 2016, Interaction of single and multiwall carbon nanotubes with the biological systems: Tau protein and PC12 cells as targets, *Sci. Rep.*, 6 (1), 26508.

[41] Seroka, N.S., Taziwa, R., and Khotseng, L., 2022, Solar energy materials-evolution and niche applications: A literature review, *Materials*, 15 (15), 5338.

[42] Nadafan, M., Tahidifar, M.R., Karimi, M., Malekfar, R., and Khorrami, G., 2018, Assessment of the optical and dielectric properties of *f*-MWCNTs/$BaTiO_3$ nanocomposite ceramics, *Ceram. Int.*, 44 (13), 15804–15808.

[43] Ahmadi, M., Zabihi, O., Nia, Z.K., Unnikrishnan, V., Barrow, C.J., and Naebe, M., 2025, Engineering flame and mechanical properties of natural plant-based fibre biocomposites, *Adv. Ind. Eng. Polym. Res.*, 8 (2), 168–195.

[44] Aziz, S.B., Brza, M.A., Nofal, M.M., Abdulwahid, R.T., Hussen, S.A., Hussein, A.M., and Karim, W.O., 2020, A comprehensive review on optical properties of polymer electrolytes and composites, *Materials*, 13 (17), 3675.

[45] Cheng, J.P., Wang, J., Li, Q.Q., Liu, H.G., and Li, Y., 2016, A review of recent developments in tin dioxide composites for gas sensing application, *J. Ind. Eng. Chem.*, 44, 1–22.

[46] El-naggar, A.M., Heiba, Z.K., Kamal, A.M., and Mohamed, M.B., 2023, Optical and dielectric behaviors of polyvinyl chloride incorporated with $MgFeO_4$/MWCNTs, *Diamond Relat. Mater.*, 138, 110243.

[47] Khan, M.T., Shkir, M., Alhouri, B., Almohammedi, A., and Ismail, Y.A.M., 2022, Modulation of optical, photophysical and electrical properties of poly(3-hexylthiophene) via Gd:CdS nanoparticles, *Optik*, 260, 169092.

[48] Dhatarwal, P., and Sengwa, R.J., 2021, Investigation on the optical properties of (PVP/PVA)/Al_2O_3 nanocomposite films for green disposable optoelectronics, *Phys. B*, 613, 412989.

[49] Kareem, A.A., 2017, Preparation and electrical properties of polyimide/carbon nanotubes composite, *Mater. Sci.-Pol.*, 35 (4), 755–759.

[50] Pratap, R., Singh, A.K., Rai, S., Mishra, A.K., Singh, J., Giri, R., and Srivastava, A., 2025, Investigations on structural, microstructural, dielectric and electrical conductivity of the ZnO-MWCNTs nanocomposite synthesized via sol-gel method, *Oxford Open Mater. Sci.*, 5 (1), itaf00651.

[51] Zidan, H.M., Abdelrazek, E.M., Abdelghany, A.M., and Tarabiah, A.E., 2019, Characterization and some physical studies of PVA/PVP filled with MWCNTs, *J. Mater. Res. Technol.*, 8 (1), 904–913.

[52] Gai, L., Zhao, H., Wang, F., Wang, P., Liu, Y., Han, X., and Du, Y., 2022, Advances in core—shell

engineering of carbon-based composites for electromagnetic wave absorption, *Nano Res.*, 15 (10), 9410–9439.

[53] Raju, V., Rani, J.V., and Basak, P., 2022, One-dimensional polythiophene/multi-walled carbon nanotube composite cathodes for rechargeable magnesium battery: Evidence of improved stability and electrochemically induced rearrangement in electrode morphology, *Electrochim. Acta*, 404, 139707.